Influence of anthropogenic aerosols on the total and spectral irradiance at the sea surface during the Indian Ocean Experiment (INDOEX) 1999

Jens Meywerk[1] and V. Ramanathan

Center for Clouds, Chemistry, and Climate, Scripps Institution of Oceanography, University of California, San Diego, La Jolla, California, USA

Received 13 October 2000; revised 4 April 2001; accepted 30 August 2001; published 4 September 2002.

[1] Unique measurements of the spectral signature of the aerosol forcing at the surface between 350 and 1050 nm wavelength during the 1999 haze event over the tropical Indian Ocean are presented and discussed. The aerosol visible optical depths reached values as high as 0.7 in the northern Indian Ocean and decreased to about 0.1 south of the Intertropical Convergence Zone (ITCZ) in the Southern Hemisphere (SH) tropical oceans. Measurements of aerosol optical depth and global (direct plus diffuse) irradiance have been taken with a grating spectroradiometer with a resolution of 3 nm onboard R/V *Ronald H. Brown*. The radiometer was calibrated onboard in real time. We inverted the direct solar spectra to obtain aerosol optical depth and to compare these with three independent sunphotometer optical depth at selected spectral intervals to assess the validity of the retrieved optical depth. We took the difference between aerosol optical depth between polluted and pristine air mass spectra to obtain the spectral signature. The difference in optical depth between the polluted regime north of the ITCZ and the pristine air masses south of the ITCZ were between 0.5 at 350 nm wavelength, 0.35 at 500 nm wavelength, and 0.1 at 1050 nm wavelength. Next, we obtained the aerosol forcing by correlating optical depth variations (for the duration of the cruise) with corresponding global irradiance variations. We found the Southern Asian aerosol reduces the solar irradiance (for a unit increase in optical depth at 500 nm wavelength) by about 25% at 350 nm decreasing to about 10% in the near-infrared. The reduction in the direct solar was a factor of 2 to 3 larger. The spectral data shown here will provide a critical test for aerosol-radiation models used for aerosol-forcing estimates. *INDEX TERMS:* 0360 Atmospheric Composition and Structure: Transmission and scattering of radiation; 0305 Atmospheric Composition and Structure: Aerosols and particles (0345, 4801); 3359 Meteorology and Atmospheric Dynamics: Radiative processes; *KEYWORDS:* aerosol, solar radiation, radiative forcing, spectral irradiance, INDOEX, spectroradiometer

Citation: Meywerk, J., and V. Ramanathan, Influence of anthropogenic aerosols on the total and spectral irradiance at the sea surface during the Indian Ocean Experiment (INDOEX) 1999, *J. Geophys. Res.*, *107*(D19), 8018, doi:10.1029/2000JD000022, 2002.

1. Introduction

[2] One of the major remaining uncertainties in determining climate change from global circulation models is the poorly understood aerosol-radiation interactions and the magnitude of the aerosol forcing at the surface and at the top of the atmosphere [*Intergovernmental Panel on Climate Change* (*IPCC*), 1995]. Aerosols can have either a cooling or a warming effect on the global climate. Whether cooling or warming dominates or even cancellation of the two effects occurs depends on a number of factors: (1) the single scattering albedo of the aerosol type, determining the portion of solar irradiance not being scattered but absorbed by the aerosol, (2) the optical depth of the aerosol, (3) the albedo of the underlying surface, (4) the vertical distribution of the aerosols, (5) the solar zenith angle, and (6) the size variation of hygroscopic aerosol particles due to changes in relative humidity [*Fraser and Kaufman*, 1985; *King et al.*, 1999]. Simply speaking low single scattering albedos result into absorption by the aerosols and hence an increase of the temperature of the layer in which the aerosol occurs if the surface reflectance is high enough (for instance over deserts or snow covered surfaces). For low surface albedos (for instance over the oceans or dark forests) even an aerosol having a single scattering value of significantly less than one can have a cooling effect since it still scatters more radiation back to space than the surface underneath. In the absence of absorption (single scattering albedo equals one), aerosols scatter parts of the solar radiation back to space, which has

[1]Now at Institute for Coastal Research, GKSS Research Center, Geesthacht, Germany.

0148-0227/02/2000JD000022$09.00

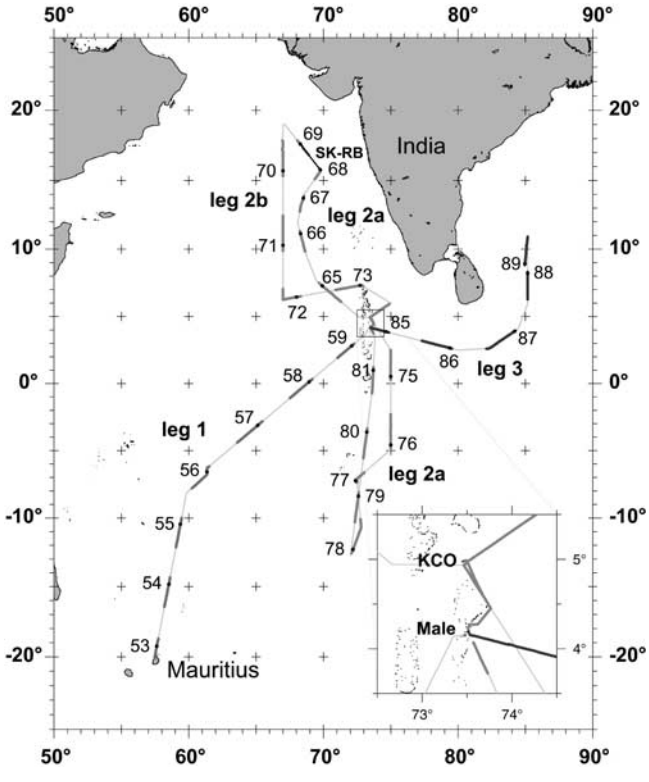

Figure 1. Cruise track of the *Ronald H. Brown* (RB) during INDOEX 1999. Daytime intervals are marked with thick pen according to the respective leg of the cruise: leg1, leg2a, leg2b, and leg3. The respective day number (day since 1 January 2001) is written next to the track, centered at 1200 UT. The area around KCO observatory and Male is enlarged in the lower right corner of the map for better orientation. The track of intercomparison with the Sagar Kanya (SK) between day 68 and 69 (10–11 March 2001) in the Arabian Sea is marked in black.

a cooling effect. This cooling effect is stronger above dark surfaces than above surfaces with high albedos. Again, the altitude of the respective aerosol layer influences the actual amount of radiation absorbed, as well as the solar zenith angle. Since natural and anthropogenic aerosols have a more or less broad and strong peak in scattering light into the forward directions, a cooling effect will be enhanced or a possible warming effect will be partly or totally compensated by absorbing aerosols at low solar altitudes [*Charlson et al.*, 1992; *Kiehl and Briegleb*, 1993].

[3] Due to the different air masses, south and north of the Inter Tropical Convergence Zone (ITCZ) the Indian Ocean is a nearly perfect laboratory for investigating anthropogenically produced aerosols and their radiative impact. In contrast to the pristine conditions in the southern part of the Indian Ocean, the northern part shows high aerosol load. Observing the aerosol radiative properties north of the ITCZ in the heavily polluted region of the Arabian Sea and south of the ITCZ enables us to extract the anthropogenically induced influence of aerosols on the solar irradiance reaching the surface.

[4] In this paper, the direct effect of anthropogenically produced aerosols over the Indian Ocean, roughly between 20°S and 20°N, 55°E and 85°E will be investigated by using data measured onboard the NOAA R/V *Ronald H. Brown* (hereafter RB) between 24 February and 31 March 1999. This was done continuously for most of the solar spectrum for both, the direct and global irradiance with different instruments. Broadband pyranometers have also been used to relate optical depth measurements to the broadband solar radiation fluxes. This combination of measurements has never been conducted in the Indian Ocean region before, except during the INDOEX First Field Phase (FFP98) [*Nguyen et al.*, 1998] between 10 February and 28 March 1998 [*Meywerk and Ramanathan*, 1999], when similar observations have been made. The observations discussed in this paper will confirm the observations done one year before and show some insights into possible interannual variations, particularly since the year 1999 witnessed much larger aerosol loading (as much as a factor of two at the Kaashidhoo Climate Observatory) (J. M. Lobert et al., Kaashidhoo Climate Observatory (KCO): A new site for observing long term changes in the tropical Indian Ocean, submitted to *Journal of Geophysical Research*, 2001) compared to 1998.

[5] In the frame of the most recent aerosol experiments the Tropospheric Aerosol Radiative Forcing Observation Experiment (TARFOX) and the Aerosol Characterization Experiment (ACE) similar observations have been made over the ocean and the direct radiative forcing has been estimated from these data sets. TARFOX [*Russell et al.*, 1997a, 1997b] focused on the determination of the direct aerosol forcing off the east coast of the United States. Several observational sites at the coast, on ships, and on aircraft have been used to determine the spectral optical depth beside many other parameters. The major field phase was from 10 July to 31 July 1996.

[6] ACE [*Raes et al.*, 2000] focused more on the chemical characterization of aerosols but included also spectral optical depth measurements. ACE-1, the first phase of the experiment was conducted in the Pacific Ocean and Southern Ocean, south of Australia, between 15 November and 14 December 1995 to investigate the aerosol plume from Australia. ACE-2 took place off the northwest African coast to sample air masses with origin of Europe and the Sahara desert.

[7] Some results from TARFOX and ACE will be compared to our results and will be discussed in the last part of this paper.

[8] Together with all other publications in this special issue, INDOEX will provide a comprehensive data set and new insights into the aerosol-radiation interaction and related aerosol chemistry in the Indian Ocean region. A detailed description of the INDOEX project and its scientific objectives are given by *Ramanathan et al.* [1996] and *Coakley et al.* [2002].

[9] The details of the ship's journey through the Indian Ocean, dates of port stays, description of the vessel, etc. are included in the overview paper on the *Ronald H. Brown* in this issue [*Dickerson et al.,* 2002] and will not be repeated here. A detailed map of the cruise track, with cross-platform intercomparison times and locations (KCO, SK-RB) may be found in Figure 1.

[10] In order to make it easier for the reader to cross compare with other papers in this issue describing data taken from the *Ronald H. Brown* we use the same notation for the

cruise track (leg1, leg2a, leg2b, leg3) as well as for the classification of the origin of air masses like Northern Hemisphere continental tropical (NHcT), Northern Hemisphere continental extratropical (NHcX), Northern Hemisphere maritime equatorial (NHmE), Southern Hemisphere maritime equatorial (SHmE), and Southern Hemisphere maritime extratropical (SHmX) as was defined in the overview paper on the *Ronald H. Brown* cruise [*Dickerson et al.,* 2002].

2. Instrumentation Used and Calibration

[11] We use the following parameters measured onboard RB:

1. Eppley PSP broadband nonventilated pyranometer: integrated global irradiance between 0.295 and 2.9 μm
2. Kipp&Zonen CM12 ventilated broadband pyranometer: integrated global irradiance between 0.295 and 2.9 μm
3. Analytical Spectral Devices (ASD) 512-channel visible to near infrared (VNIR) grating spectroradiometer: (1) global spectral irradiance between 0.35 and 1.05 μm wavelength; and (2) direct solar irradiance between 0.35 and 1.05 μm wavelength
4. Two Microtops II sunphotometers: (1) aerosol optical depth at 380, 440, 500, 675, 870 (instrument #1, S/N 4072) and 1020 nm (instrument #2, S/N 3685) wavelength; (2) integrated ozone columnar content (instrument #2, S/N 3685); and (3) integrated water vapor columnar content (instrument #2, S/N 3685).

[12] All instruments listed under 1, 2 and 3a were mounted on top of a tower, approximately 10 m above the foredeck on gimbaled frames in order to compensate for the pitch and roll of the ship. The remaining tilt of the sensor surfaces was estimated by observing the remaining movement of the gimbal surfaces for typical sea state conditions during the cruise to be less than ±2° for the small pitch and roll of the vessel in the low wind regime of the tropical region. In the worst case (without atmosphere, 100% of the radiation comes directly from the Sun) a tilt of ±2° of the sensor surface would result in an error of about −0.06% for overhead sun, ±2.1% at 30° zenith angle, ±6.5% at 60° and ±24.8% at 80°. Since about only 85–90% (depending on the wavelength and the aerosol optical depth) of the solar irradiance are from the direction of the Sun and the diffuse skylight is more uniformly distributed over the sky, the error due to a tilted surface is less than the above mentioned values, depending on wavelength and aerosol load. Since scattering is higher for shorter wavelengths (Rayleigh and Mie, depending on particle size) the error due to the tilted surface is smaller for shorter wavelengths. For increasing aerosol optical depth the error due to the sensor tilt decreases, since the main contribution to the error, the changes in direct solar beam get slightly weaker. The hemispherically integrated measured parameters have been monitored continuously throughout the cruise. The maximal possible error is also reduced if one considers only data from a certain solar zenith angle range as done in this study. Only data from solar zenith angles between 0° and 36° are analyzed here to derive the spectral forcing.

[13] Parameters listed under 3b and 4 have been measured approximately once every hour during daytime (see Figure 1 for daytime periods during the cruise), whenever cloudiness permitted. These measurements have been done hand-held, since the ship did not provide a sufficiently accurate automatic sun tracking system. An average of 10 hand-held spectra out of 100–200 taken subsequently during a 1.5–3 min period was assumed to represent the direct irradiance when the standard deviation of those 10 spectra was below 0.5%. This is very similar to the procedure used by the built-in software of the Microtops II sunphotometer used to determine the direct irradiance.

[14] Optical depth, water vapor, and ozone columnar content measurements are in general usable, from all observations, even under partially cloudy conditions, provided the solar disc was not obscured by clouds (even cloud edges or thin cirrus). However, broadband global irradiance from the pyranometers and the spectral global irradiance from ASD are only meaningful if the entire sky was cloudless or at least the influence of enhanced diffuse radiation due to scattered clouds is negligible. Even fragments of clouds (especially convective clouds close to the solar disc, but not obscuring it) can increase the global solar irradiance due to their edges, reflecting radiation onto the instruments sensor in addition to the undisturbed direct beam irradiance. This so-called 'lens effect' would result in an increased global irradiance and hence would mask the aerosol influence on the surface irradiance. Shortly before the solar disk is shaded by a bypassing cumulus cloud, the hemispherically integrated irradiance can considerably increase above its clear sky value. For extreme cases, the measured global irradiance can even exceed the extraterrestrial irradiance of 1365 W m^{-2} [*Meywerk*, 1997; *McCormick and Sührcke*, 1990]. This effect can be very critical while estimating the direct influence of aerosols on the hemispherically integrated (global) irradiance whenever clouds are in the sky. To rule out these cases, sky photographs with a wide-angle lens have been taken throughout the experiment once every hour and have been analyzed.

[15] In the following the calibration of each instrument will be described. The full, detailed accuracy estimate of all instruments mentioned here can be found in the work of *Meywerk and Ramanathan* [1999] and will not be repeated in detail here.

2.1. Pyranometers

[16] For this study we have used a redundant set of broadband pyranometers in order to ensure the accuracy of the spectrally and hemispherically integrated solar irradiance, and to rule out possible biases due to any offset in calibration coefficients of a single instrument. The linear correlation between the two instruments using about 65000 simultaneously taken 10 s averages is:

$$I_E = 0.9875\left(\pm 1.29 \times 10^{-4}\right) I_K + 5.81\left(\pm 8.17 \times 10^{-3}\right)$$

with I_E denoting the irradiance measured by the Eppley PSP instrument and I_K denoting the irradiance measured by the Kipp&Zonen CM12. The Eppley gives slightly smaller values than the Kipp&Zonen but with a positive offset, partly reducing this underestimation at higher irradiance (above 464 W m^{-2}). At lower irradiances the positive offset of the Eppley dominates. Total cancellation of the statistical difference between these instruments is at 464 W m^{-2}. A 0.68% uncertainty in these data at 1000 W m^{-2} and a 4.5%

uncertainty at 100 W m^{-2} needs to be considered from this statistical analysis. Since we are only using data from the pyranometers for clear sky and low solar zenith angles (high irradiances), the difference between the readings of the two instruments is minimal in our study.

[17] This intercomparison of the two instruments rules out any major systematic difference between the instruments in spite of the fact that the instruments are from different manufacturers, have different sensitivities and one of them has been ventilated to reduce the outer filter domes thermal emission to the sensors surface. Apparently the "natural" ventilation of the unventilated instrument due to the movement of the ship and the wind was sufficient to reduce this kind of error. Both pyranometers have been factory calibrated immediately before the cruise by comparison with a 1000 W NIST-traceable standard lamp.

2.2. ASD Spectroradiometer

[18] The ASD spectroradiometer [*Curtiss and Goetz*, 1997] has been factory calibrated before the cruise and 5 times during the cruise using a LICOR portable calibrator [*Licor*, 1990], by comparing the known spectrum of a 200 W NIST-traceable calibrated tungsten lamp to the readings (digital numbers, DN) of the spectrometer. We are aware, however, of the general problems related to this type of calibration procedure as described by *Kiedron et al.* [1999], but we had to follow this way of calibration, since we were not able to carry out Langley calibration which requires long term (at least an entire solar day) observation under very stable atmospheric conditions, which are usually only found at high altitude locations. However, calibrations with this type of setup we used, were found to be least problematic [*Kiedron et al.*, 1999] compared to others.

[19] We corrected the readings of the spectroradiometer also for the cosine response error of the Delrin diffuser used for the spectral global irradiance measurements with the ASD. A slightly wavelength and strong angle dependent correction had to be applied to the global spectral irradiance data which peaks at 55° zenith angle (12% overestimation at 600 nm wavelength) and drops to an underestimation of about 20% at 80°. This cosine error characterization of the diffuser has been done on an optical table before the cruise. It was also found that the pipe, narrowing the field of view from 180° to 2° instead of narrowing to about 0.53° (solar disc) for taking direct beam measurements did not significantly influence the determination of the optical depth (underestimation of only 1.3–2.5% depending on the wavelength interval). During the intensive field phase the calibration procedure and data correction were the same as done during the First Field Phase 98 (FFP) and will not be repeated here. Details about the calibration procedure and estimation of uncertainties can be found in the work of *Meywerk and Ramanathan* [1999].

[20] In contrast to the 1998 FFP data we observed a wavelength dependent drift in the calibration coefficients during this cruise, most likely caused by a degradation of the sensor material due to the long and repeated exposure of the sensor material (photodiode array) to the solar radiation. In general, the observed drift was more pronounced and negative for shorter wavelengths and less pronounced and positive for longer wavelengths. The actual numbers may be seen in Table 1. A reduction in calibration coefficients represents an underestimation of the measured irradiance (overestimation of optical depth) and vice versa. If this drift had not been corrected for, not only the magnitude of measured irradiance would have been affected, but also the spectral dependence of all derived parameters. The calibration coefficients for the period between two calibrations have been obtained by interpolation.

Table 1. Observed Percentage Difference in Calibration Coefficients at the Beginning and Towards the End of the Cruise at Different Wavelengths[a]

	350 nm	400 nm	600 nm	900 nm
Global	−21.6	−2.7	+7.9	+3.6
Direct	−25.6	−4.6	−0.9	+2.1

[a] A reduction in calibration coefficients represents an underestimation of the measured irradiance and vice versa.

[21] The combined measurement error of the ASD is estimated to be less than 2% between 500 and 950 nm and below 6% between 380 and 500 nm and 950–1050 nm [*Meywerk and Ramanathan*, 1999]. Since in this study a time-dependent calibration coefficient set has been used (instead of an average calibration coefficient set used in the earlier study) the error mentioned above is considered an upper limit. The manufacturer states an accuracy of the instrument between 400 and 900 nm wavelength of 5% (ASD Technical Guide) for irradiance calibration using the calibration procedure described above.

2.3. Microtops II

[22] We have used two different Microtops II sunphotometers during the cruise for hand-held measurement of the aerosol optical depth and the water vapor and ozone columnar content.

[23] The first instrument (S/N 3685) estimating the ozone columnar content by measurement of the direct beam solar irradiance at 300, 305.5 and 312.5 nm and the water vapor columnar content by measuring the direct irradiance at 936 and 1020 nm with a full width at half maximum of 10 nm for the latter two channels, respectively. The water vapor algorithm for this instrument was developed by *Reagan et al.* [1987] and evaluated by *Michalsky et al.* [1995]. The built-in calibration routine automatically corrects for Rayleigh optical depth in the ultraviolet and visible wavelength regions, using the Rayleigh coefficients derived by *Penndorf* [1957]. The surface pressure needed for that parameterization is measured directly by the instrument, and the latitude, longitude and time information needed to calculate the solar zenith angle are automatically read from a Global Positioning System (GPS) receiver connected to the Microtops sunphotometer. The instrument also automatically corrects for the aerosol optical depth in the water vapor channel at 940 nm using the optical depth measured in the 1020 nm water vapor absorption free channel assuming that the optical depth is constant with wavelength between these two channels.

[24] The second instrument (S/N 4072) was designed to derive the aerosol optical depth from measurement of the direct beam irradiance at 380, 440, 500, 675, and 870 nm. These optical depth measurements have also been automatically corrected for Rayleigh attenuation in all wavelengths as described above. The ozone Chappuis-band optical depth

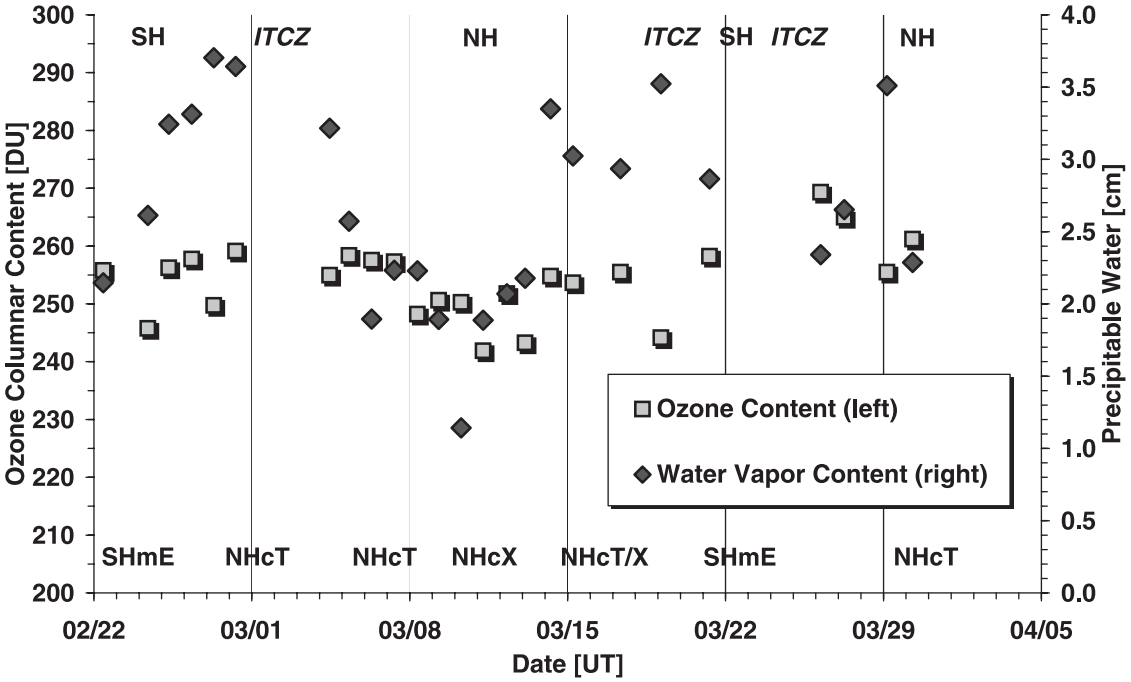

Figure 2. Time series of the water vapor columnar content (right axis, in cm precipitable water) and the ozone columnar content (left axis, Dobson Units) derived from the Microtops II sunphotometer S/N 3685 for the entire cruise along the cruise track. The ozone data has been used to correct optical depth measurements of the ASD for the absorption in the Chappuis band. At the top of the plot a rough estimate of the location of the vessel is indicated: SH, Southern Hemisphere; ITCZ, Intertropical Convergence Zone; NH, Northern Hemisphere.

has been subtracted using the ozone columnar content measurements from above, together with the ozone absorption coefficients from *Molina and Molina* [1986].

[25] Both instruments use a photodiode set as detectors topped with different interference filters. They have been absolutely calibrated using Langley technique right before and after the cruise at Mauna Loa calibration facility, Hawaii, with no change observed between these two calibrations. The manufacturer states a 1–2% precision for this instrument after the careful Langley calibration and repeatability of 0.5%.

2.4. Optical Depth Calculation From Direct Beam ASD Measurements

[26] The optical depth is defined through the Lambert-Beer law for monochromatic radiation:

$$I = I_0 e^{-\tau}$$

with I being the direct normal irradiance measured at the surface, I_0 being the extraterrestrial irradiance [*Kurucz*, 1992] and τ the total optical depth from all atmospheric constituents including aerosols. τ can also be written as the sum of optical depths caused by different constituents as

$$\tau = \tau_{Ray} + \tau_{Abs} + \tau_{Aer}$$

with the indices *Ray*, *Abs*, and *Aer* denoting the Rayleigh optical depth (molecular scattering), *Abs* the optical depth due to gaseous absorption like in the ozone Chappuis band (0.4–0.7 μm), several water vapor and O_2 absorption bands, and *Aer* denoting the optical depth of aerosols (Mie scattering and absorption if the single scattering albedo is less than 1).

[27] The Rayleigh extinction has been parameterized and subtracted from the total optical depth for the known surface pressure [*Penndorf*, 1957; *Leckner*, 1978]. The ozone optical depth in the Chappuis band has been corrected for since the ozone columnar content is known. We took the columnar content of ozone from the Microtops measurements (Figure 2) described below and the respective ozone absorption coefficients from *Molina and Molina* [1986] and *Leckner* [1978]. The absorption bands of water vapor and O_2 have not been corrected for, since they are either negligible or can be easily identified by the position of their respective centers (see Figures 5a and 5b). Figure 2 displays the time series of ozone columnar content (gray squares, left axis, in Dobson Units), and the water vapor columnar content (black diamonds, right axis, in cm) from Microtops measurements throughout the cruise. While the ozone content remained relatively stable and low in the study area (20°S–20°N), the water vapor content varied considerably with lowest values at the northernmost (Arabian Sea) and southernmost (Mauritius) positions and highest values close to the ITCZ. The ozone columnar content has been used to correct the optical depth measurements for the ozone absorption in the Chappuis band.

[28] With these corrections applied it is possible to calculate the aerosol optical depth for the entire spectrum between 0.35 and 1.05 μm. Figures 3a and 3b display the time series of optical depth measurements from Microtops sunphotometer and ASD measurements, respectively. For both instruments three different wavelength bands in the visible and near infrared have been chosen for intercomparison (Microtops

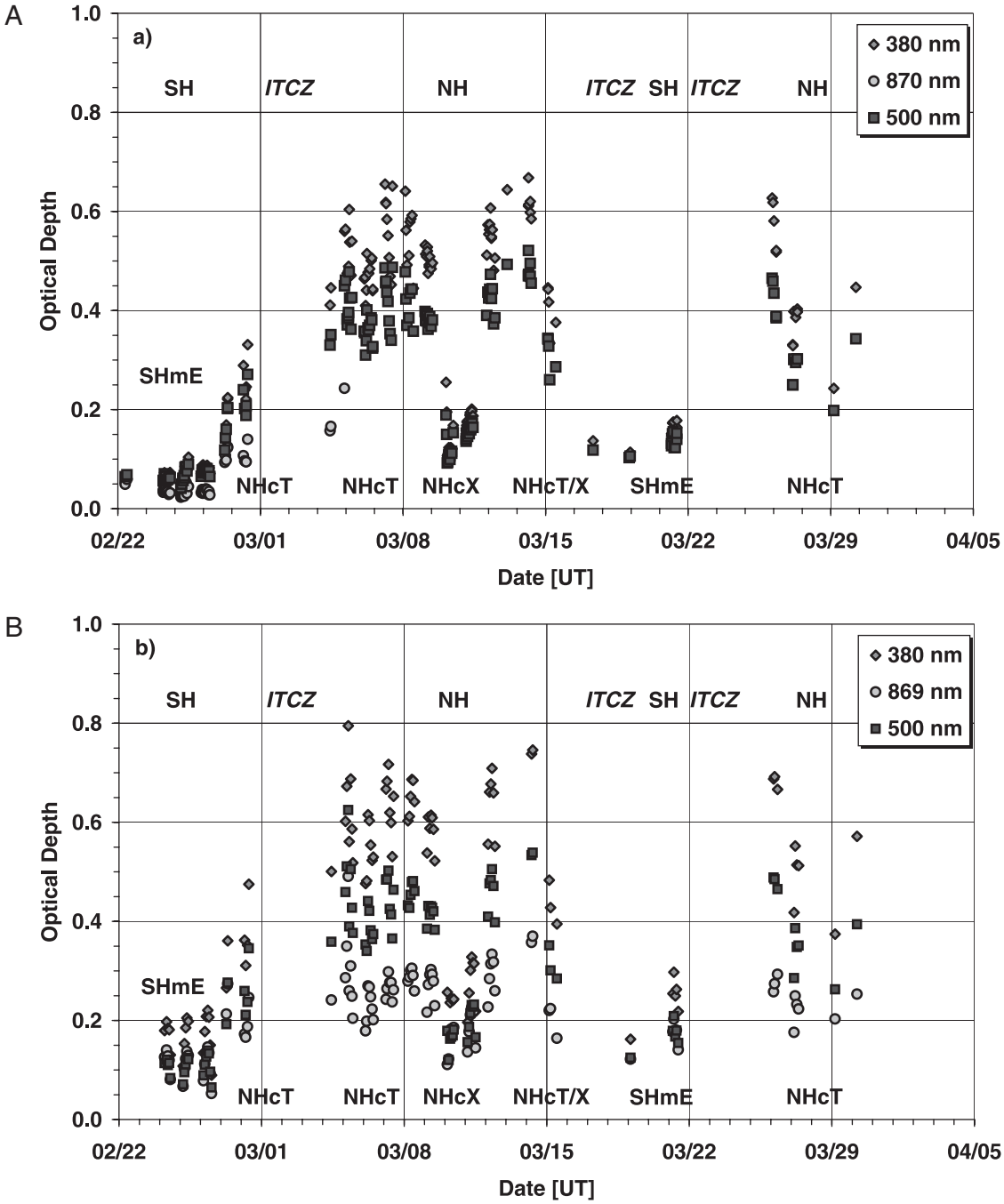

Figure 3. In the lower part of the plot the origin of the respective air mass is indicated (see text for explanation). (a) Time series of optical depth at 380, 500, and 870 nm wavelength from Microtops measurements along the cruise track of *Ronald H. Brown*. (b) Time series of optical depth at 380, 500, 870 nm wavelength from ASD spectrometer along the cruise track of *Ronald H. Brown*. At the top of each plot a rough estimate of the location of the vessel is indicated: SH, Southern Hemisphere; ITCZ, Intertropical Convergence Zone; NH, Northern Hemisphere.

S/N 3685: 380, 500, 870 nm; ASD 927: 380, 500, 870 nm). In the upper part of the respective panel a coarse estimate of the geographical position of the vessel is given: SH, Southern Hemisphere, ITCZ, Inner Tropical Convergence Zone, NH, Northern Hemisphere. The acronyms on the lower end of the panel stand for the respective origin of the air masses mentioned earlier, derived from back-trajectory calculations and measurements of various chemical compounds, respectively [*Dickerson et al.*, 2002; *Mühle et al.*, 2002]. In general, low values of optical depth are observed in the Southern Hemisphere (SH) with only little wavelength dependence and highest values are observed in the northern hemisphere with strong dependence on wavelength, except at the northernmost position in the Arabian Sea, when air masses originated from Saudi Arabia rather than the Indian subcontinent.

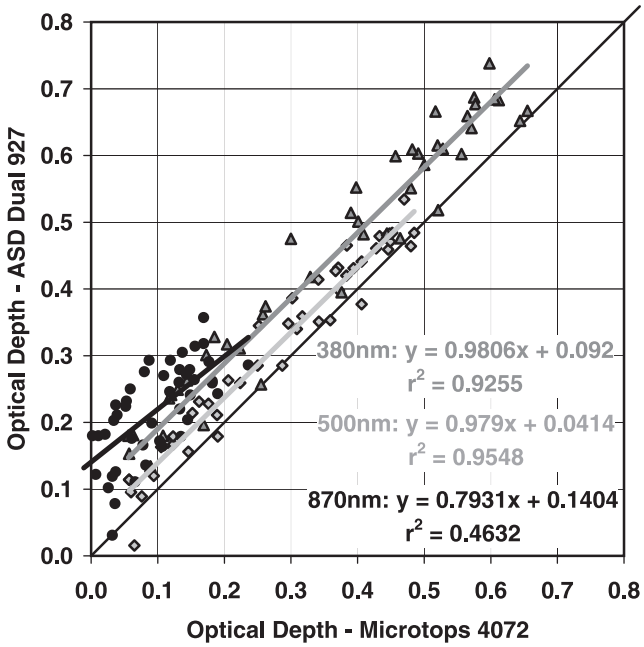

Figure 4. Intercomparison of Microtops optical depth (S/N 4072) and optical depth inferred from the ASD spectrometer for all nearly simultaneously taken measurements and the respective linear fits for the three wavelengths 380, 500, and 870 nm.

[29] The intercomparison of optical depths inferred from ASD and Microtops is shown in the scatterplot in Figure 4 for the three different wavelength bands. In general, the optical depth inferred from the ASD is slightly biased to higher values compared to the optical depths from Microtops (gain −2%, +0.09 offset at 380 nm, −2.1% gain, +0.04 offset at 500 nm and −21% gain, +0.14 offset at 870 nm). The manufacturer of the ASD spectroradiometer states an accuracy of 5% for most wavelengths (400–900 nm) for irradiance measurements, which translates into an accuracy of 0.049 in optical depth. The intercomparison of optical depth from the two instruments in the near infrared wavelength band at 870 nm is poor. The ASD shows higher optical depths at shorter wavelengths, resulting in a weaker spectral dependence of optical depth (smaller Ångstrøm exponent). Microtops reports an absolute accuracy of their instrument of 0.02 in optical depth for the visible channels. This comparison, however, is still within the range of precision reported by the manufacturers of the respective instruments. A more comprehensive intercomparison of a total of six identical Microtops sunphotometers (including our instruments) carried out by different groups on the vessel, equipped with the same channels was conducted. This intercomparison was done throughout the cruise by taking simultaneous measurements of the optical depth, covering a wide range of optical depth measurements. The differences between ASD and our Microtops instrument are at the same order of magnitude as the intercomparison between all six Microtops instruments (J. Welton, 2000). A cross comparison with that study suggests a good agreement and reliability of all available optical depth measurements from the vessel.

[30] The optical depth derived from ASD measurements for a fairly pristine day (24 February 1999, NHmE regime) and a rather polluted day (7 March 1999, NHcT) are shown in Figures 5a and 5b, respectively. The absorption bands of water vapor and molecular oxygen can be clearly identified and are not to be interpreted as pure aerosol features. The diurnal variation of the optical depth at 500 nm is overlaid in the upper left corner of the respective plot.

[31] On 24 February, five measurements have been taken spread over the entire day between 0546 and 1233 UT. The aerosol optical depth was in general very low with little variation and almost no dependence on wavelength (Ångstrøm exponent close to 0), suggesting a small number of large particles (sea salt). The spectral optical depth on 7 March was very high with large variance from about 0.35 to 0.51 at 500 nm wavelength and fairly pronounced spectral dependence (0.75 at 350 nm to 0.35 at 675 nm, Ångstrøm exponent about 1.2).

[32] The strong variation of optical depth in the 350–410 nm region originates from the combination of variation in extraterrestrial irradiance (narrow Fraunhofer emission lines of the solar photosphere) *Labs and Neckel* [1968] with the bandwidth of the spectroradiometer (3 nm) and the uncertainty in wavelength calibration of the instrument, which is given by the manufacturer to be (1 nm) with a repeatability of 0.1 nm.

[33] The difference between the two graphs can be taken as the anthropogenic signal induced by the aerosol optical depth due to the mixture of sulfate, soot, organics and mineral dust from human activity, transported to the Indian Ocean area. The relative humidity in the boundary layer and above was low and similar on both days (from radiosonde observations not shown here), so the effect of humidity growth related changes of the boundary layer aerosol can be considered small. The total columnar water vapor content on 24 February (2.6 cm) was only slightly higher than on 7 March (2.2 cm), mostly since on 24 February the water vapor content above the boundary layer was slightly bigger but the relative humidity above the boundary layer for both days was around 80% at the most, which can be considered a relative humidity were small changes in relative humidity are not leading to major particle growths and related changes in scattering coefficients. For instance a change in relative humidity from 60% to 70% would result in an enhanced scattering due to particle growth of about 10%, a change of relative humidity change from 70% to 80% would increase the scattering coefficient by about 17% [*Clarke et al.*, 2002]. Considering a fixed particle number density and a fixed geometrical thickness of the aerosol layer this would result in a 10% and 17% increase in optical depth, respectively. The corresponding uncertainty in the estimated optical depth ranges from 0.05 to 0.08 at 500 nm on the polluted day, and from 0.01 to 0.02 on the pristine day. From the above we consider the difference found in optical depth (Figure 5c) not to be dominated by relative humidity change related scattering coefficient increases, but dominated by anthropogenic aerosol.

[34] For clear sky conditions the increase in optical depth due to anthropogenically produced aerosols is significantly bigger due to pollution with a strong spectral dependence

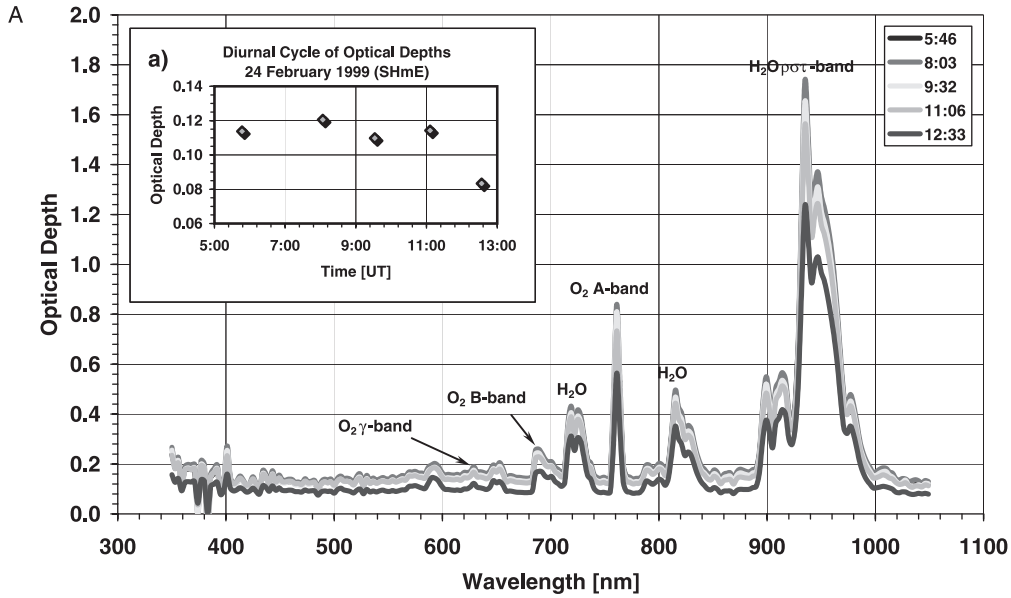
A
a)
Diurnal Cycle of Optical Depths
24 February 1999 (SHmE)
Optical Depth
Time [UT]
5:46
8:03
9:32
11:06
12:33
$H_2O\rho\sigma\tau$-band
O_2 A-band
H_2O
H_2O
O_2 B-band
$O_2\gamma$-band
Optical Depth
Wavelength [nm]

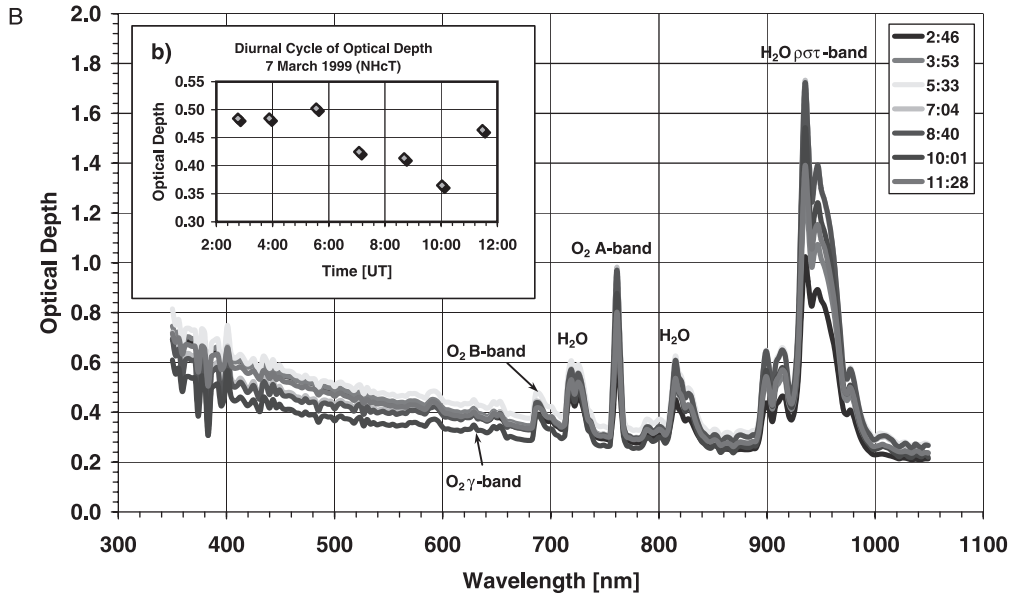
B
b)
Diurnal Cycle of Optical Depth
7 March 1999 (NHcT)
Optical Depth
Time [UT]
2:46
3:53
5:33
7:04
8:40
10:01
11:28
$H_2O\rho\sigma\tau$-band
O_2 A-band
H_2O
H_2O
O_2 B-band
$O_2\gamma$-band
Optical Depth
Wavelength [nm]

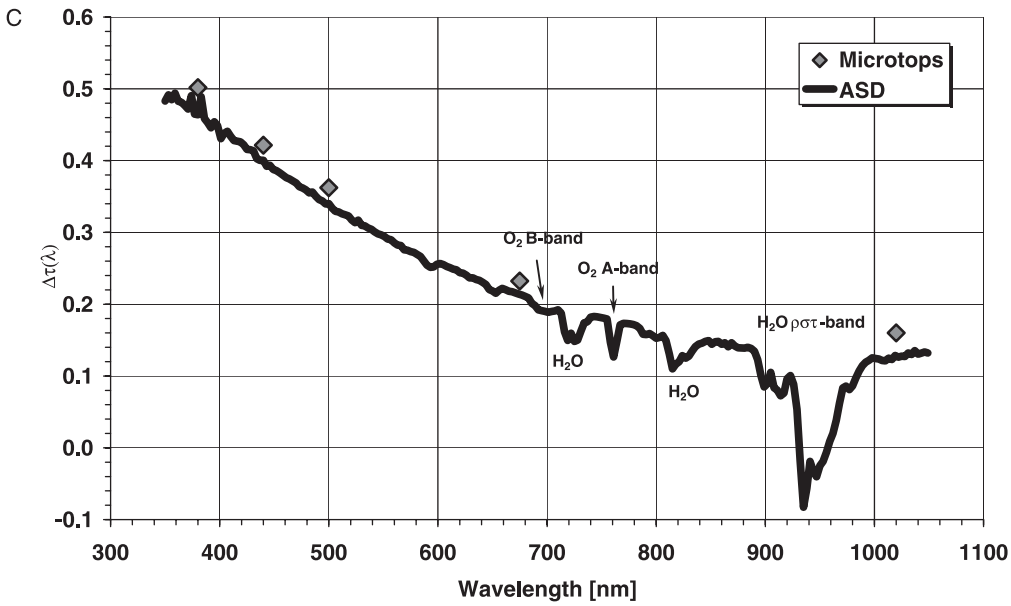
C
Microtops
ASD
O_2 B-band
O_2 A-band
$H_2O\rho\sigma\tau$-band
H_2O
H_2O
$\Delta\tau(\lambda)$
Wavelength [nm]

(optical depth of 0.5 at 400 nm and 0.2 at 680 nm), suggesting a smaller effective radius of the aerosol as compared to the pristine conditions. Figure 5c shows the difference between the daily averages from Figures 5a and 5b as inferred from ASD and Microtops measurements. The daily average for the polluted and pristine day have been calculated and the difference between the polluted day spectral optical depth and the pristine day's optical depth is displayed. This difference can be interpreted as the change in optical depth due to the pollution from the Indian subcontinent. The optical depth is increased by as much as 0.5 at 350 nm wavelength, 0.35 at 500 nm, and 0.13 at 1000 nm. In this difference plot the strong water vapor absorption bands can still be identified, since the columnar water vapor content was not the same at the two respective days. On the most polluted day the integrated water vapor content inferred from Microtops measurements was much less (7 March 1999, 2.2 cm) than on the pristine day (24 February 1999, 2.6 cm) (see Figure 2). The same is true for the oxygen A-band which can still be located in the optical depth difference plot. The surface pressure was about 4 hPa higher on the pristine day (1005–1008 hPa), resulting in a slightly stronger absorption in the oxygen band compared to the polluted day (1001–1003 hPa). Again, these remaining absorption band features are not to be interpreted as pure aerosol features. They do exhibit, however, that in the visible part of the spectrum, not only aerosols impact the clear sky irradiance, but also changes in water vapor columnar content and to a smaller extend surface pressure (air mass) might have a nonnegligible impact in certain spectral regions.

[35] Compared to earlier measurements taken during INDOEX 1998, the aerosol optical depth was not found to be significantly higher during this cruise. A very much pronounced increase from 1998 to 1999 was observed from optical depth measurements taken at the Kaashidhoo Climate Observatory (KCO) [*Satheesh and Ramanathan*, 2000]. They observed an increase in average optical depth at 500 nm wavelength from 0.16 during February – March, 1998 to 0.41 during the same period in 1999. This strong increase in aerosol optical depth from 1998 to 1999 can not be confirmed by our measurements at various locations in the Indian Ocean and the Arabian Sea from the Sagar Kanya in 1998 and the data presented here. We already observed maximum optical depth in the Arabian Sea in 1998 [*Meywerk and Ramanathan*, 1999] of up to 0.55 at 500 nm wavelength and found these values confirmed in 1999 in the same area.

3. Intercomparison With Other Sources of Data

[36] Two intercomparisons have been conducted during the cruise: The first intercomparison with the Kaashidhoo Climate Observatory (KCO) located at 4°57.9′N, 73°27.9′E, has been conducted for a 23 hour period from 5 March 0000 (shortly after sunset) through 2300 UT (4 March, 2000 through 5 March, 1900 LT, shortly before sunset). An entire solar day was covered and available for intercomparison. AOD measurements have been taken from the KCO site using a hand-held Microtops sunphotometer (S/N4073, 380, 440, 500, 675 and 870 nm) equipped with the same channels as the one used on the *Ronald H. Brown*. An ASD instrument has been used to monitor both, the direct and global spectral irradiance continuously in 512 channels between 350 and 1050 nm. The intercomparison for the time period mentioned above is not shown here, since the sky was temporarily covered with thin cirrus clouds (this has been supported by sky photographs), thus making it hard to intercompare the optical depths measurement from the different locations, even though close together. However, a coarse trend could still be seen in all observations: the optical depth at 500 nm wavelength increased from 0.3 at 0200 UT to about 0.45 at 0400 UT. Later an increase in optical depth from about 0.4 at 0600 UT to about 0.5 at 1100 UT could be identified. During the intercomparison the *Ronald H. Brown* was located on a nearly fixed position (73°29.1′E, 4°57.7′N) ESE of the KCO observatory at a distance of about one nautical mile from the island, heading into the wind blowing from NNE (20° at 4–2 ms^{-1} decreasing with time). The ASD instruments at KCO and the one used on the ship have been intercompared side by side before the INDOEX field phase and showed an agreement of 2% in irradiance.

[37] The second intercomparison was conducted between the Sagar Kanya, owned by the Department of Ocean Development (DOD), Government of India, and the *Ronald H. Brown* for a 24 hour period from 9 March, 1100 UT through 10 March, 1130 UT, while the ships were steaming northward during leg 2a (see Figure 1, SK-RB, day 68–69), side by side, but not contaminating each others sample air masses with their stack gases. This intercomparison is shown in Figure 6 for all available instruments (Microtops II (S/N 3685 & S/N 4072) the ASD instrument on *Ronald H. Brown* and the DOD hand-held sunphotometer operated on board the Sagar Kanya). The instrument used on Sagar Kanya is a 5 channel (399, 497, 667, 848 and 1051 nm) photodiode sunphotometer developed by the Physical Research Laboratory in Ahmedabad, India. This instrument had already been used during several pre-INDOEX cruises between 1996 and 1999 and is described in more detail in *Jayaraman et al.* [1998] with the results from INDOEX Intensive Field Phase 1999 (IFP99) in the work of *Jayaraman et al.* [2001].

[38] The agreement in optical depth at the wavelength 380, 500 and 675 nm is within the 0.05 precision stated by the manufacturers of the respective instruments for the higher optical depth values on 9 March and within 0.1 for low optical depths on 10 March. The low optical depth values found in this part of the Arabian Sea can be considered unique, since usually this area is highly polluted by air from India. However, back-trajectory analysis for the position of the *Ronald H. Brown* suggests that the air masses origin on 10–11 March was from the Saudi Arabian peninsular rather than from the Indian subcontinent with very low aerosol burden but still slightly above the values found in the Southern Hemisphere pristine conditions,

Figure 5. (opposite) Spectral optical depth for (a) a pristine day (24 February 1999) inferred from ASD, (b) a rather polluted day (7 March 1999) inferred from ASD, and (c) difference in average optical depths from (b) and (a) together with the same difference in optical depth inferred from Microtops measurements.

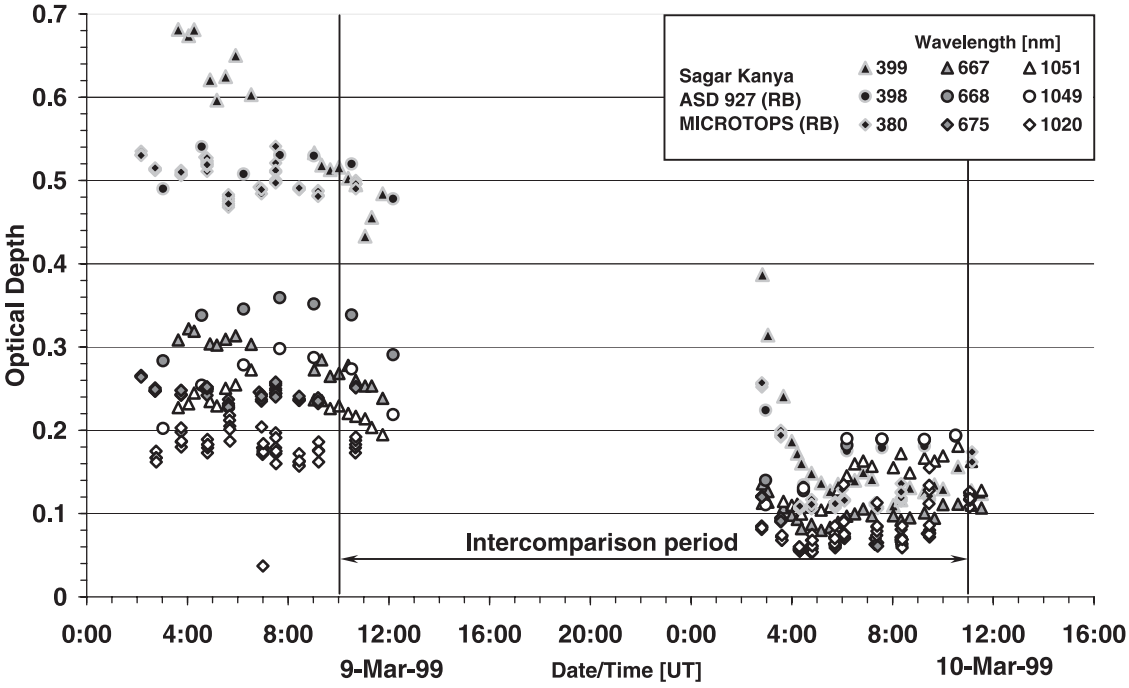

Figure 6. Intercomparison of optical depth measurements with the Sagar Kanya from 9 March, 0800 UT to 10 March, 2400 UT.

SHmE (compare Figures 5a and 5b) [*Dickerson et al.*, 2002; *Mühle et al.*, 2002].

4. Correlation Between Global Irradiance and Optical Depth

[39] In this chapter, the influence of increased aerosol optical depth on the global irradiance, integrated over all solar wavelength bands and for certain spectral intervals is investigated using data from the pyranometers, the ASD direct beam and global irradiance measurements as listed above as 1, 2 and 3, respectively.

[40] For an estimation of the effect of aerosols on the irradiance at the surface, the integrated global irradiance from broadband pyranometer measurements (0.295–2.9 μm), the integrated 400–700 nm irradiance from the ASD spectroradiometer have been plotted versus the observed optical depth at 500 nm. In order to minimize scattering due to different geometries, only data have been plotted from global measurements for which $\mu = \cos(\theta) \geq 0.8$ ($\theta \leq 36°$), with θ being the solar zenith angle. These measurements have also been normalized with μ. The slopes of irradiance versus optical depth in the respective plots are a measure of the reduction of irradiance due to increased optical depth for nearly overhead sun conditions. Figure 7 shows the broadband pyranometer data versus the optical depth at 500 nm measured with the ASD spectrometer (diamonds) and the Microtops instrument (circles). The large scatter in the pyranometer data is a result of the influence of varying water vapor (720 nm band, 820 nm band and $\rho\sigma\tau$-band, compare Figure 2) toward the upper end of the visible and the near infrared part of the spectrum and remaining uncertainties due to not completely clear skies. To minimize the errors due to non completely clear skies, only pyranometer data have been used, when the standard deviation of the pyranometer data in a 10 min time frame around the respective optical depth measurement was less than 5%. A rapid change in irradiance would mean either an obstruction of the solar disc by thin clouds or a rapid increase in irradiance due to cloud edge reflections. To filter out the influence of varying water vapor content on absorption it would be necessary to bin the measurements into groups with the same or similar water vapor content but varying optical depth. This was not possible since the number of samples is much too small for such a detailed statistical analysis. With these uncertainties in mind we find a forcing of -15.7 W m^{-2} per increase of 0.1 in optical depth at 500 nm for low solar zenith angles from ASD measurements and -14.7 W m^{-2} in solar irradiance from Microtops measurements. Here, we intentionally use the dependence of irradiance due to an increase of 0.1 in optical depth rather than unit, since the dependence of irradiance on changes in optical depth is not necessarily linear with increasing optical depth for large optical depths. It should be noted here, that this presumed linear dependence is only valid for the range of optical depth investigated in this paper (0.05–0.7 at 500 nm).

[41] The scatterplot for the integrated 400–700 nm global irradiance from ASD measurements versus optical depth is shown in Figure 8. Due to the negligible influence of varying water vapor in this spectral band the scatter in this plot is much less than for the pyranometer flux. Again, an average of the 400–700 nm flux has only been used, if the respective standard deviation within a 10 min time frame around the corresponding optical depth measurement was less than 5% of the irradiance. Also shown on the same plot is the direct beam 400–700 nm irradiance as measured by the ASD instrument. The scatter in the direct irradiance slope is minimal, since no uncertainties must be expected in the direct irradiance from cloud edge reflections, as it is

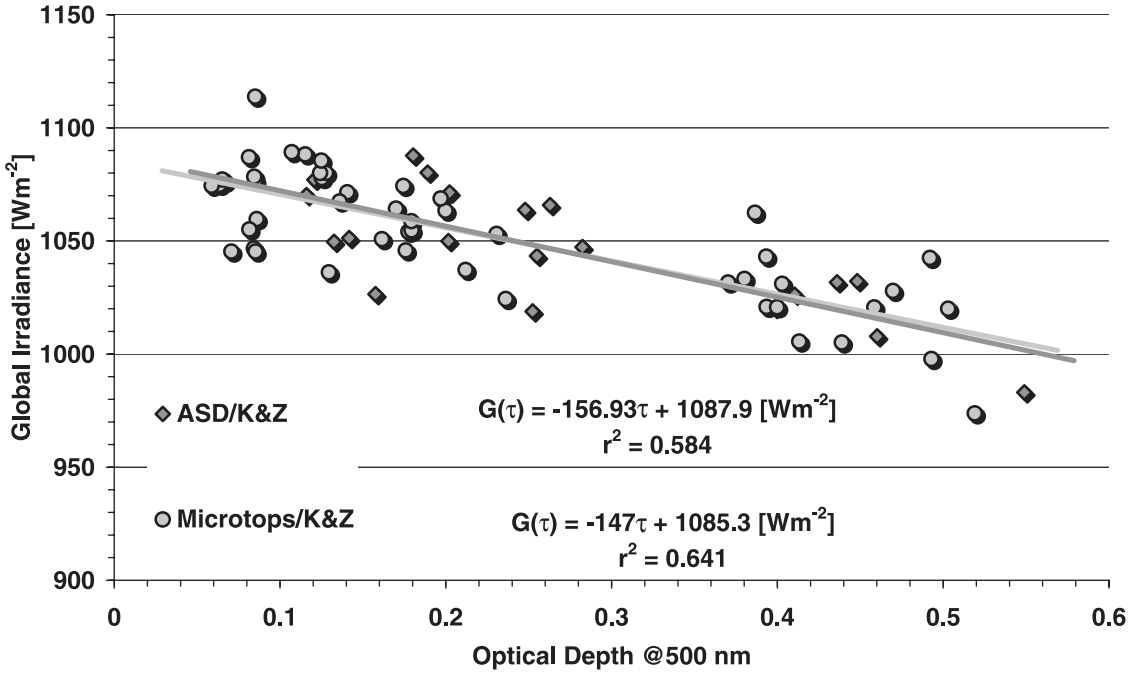

Figure 7. Broad band pyranometer data (K&Z) versus optical depth at 500 nm from ASD and Microtops and the respective linear fits.

seen in the global irradiance measurements (ASD-global and pyranometer). The slopes are overlaid to the graph: a -9.0 W m^{-2} reduction was found for the global irradiance in the 400–700 nm band observed per 0.1 increase in optical depth at 500 nm, and a -28.8 W m^2 reduction in the direct beam 400–700 nm band, respectively.

[42] Since we have the complete spectral information between 350 and 1050 nm we can go beyond the spectrally integrated slopes presented above and calculate the slopes of the irradiance versus optical depth at 500 nm not only for those broad spectral bands, but also for each of the spectral channels of the instrument in units W m^{-2} nm^{-1}. This is shown in Figure 9 for the global and direct beam measurements (solid black and gray lines, left side axis). The slopes are highly correlated with the intensity of incident solar radiation at the respective wavelength, as can be seen

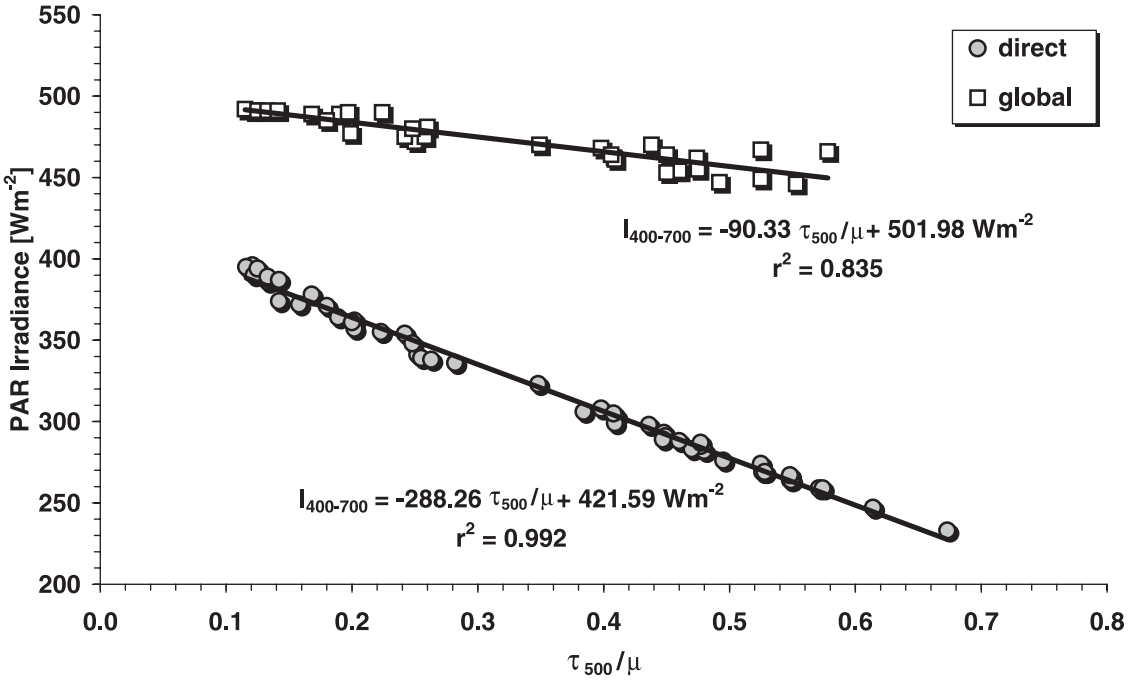

Figure 8. Scatterplot of the integrated 400–700 nm, photosynthetically active radiation (PAR) global and direct irradiance from ASD versus the optical depth at 500 nm inferred from ASD measurements.

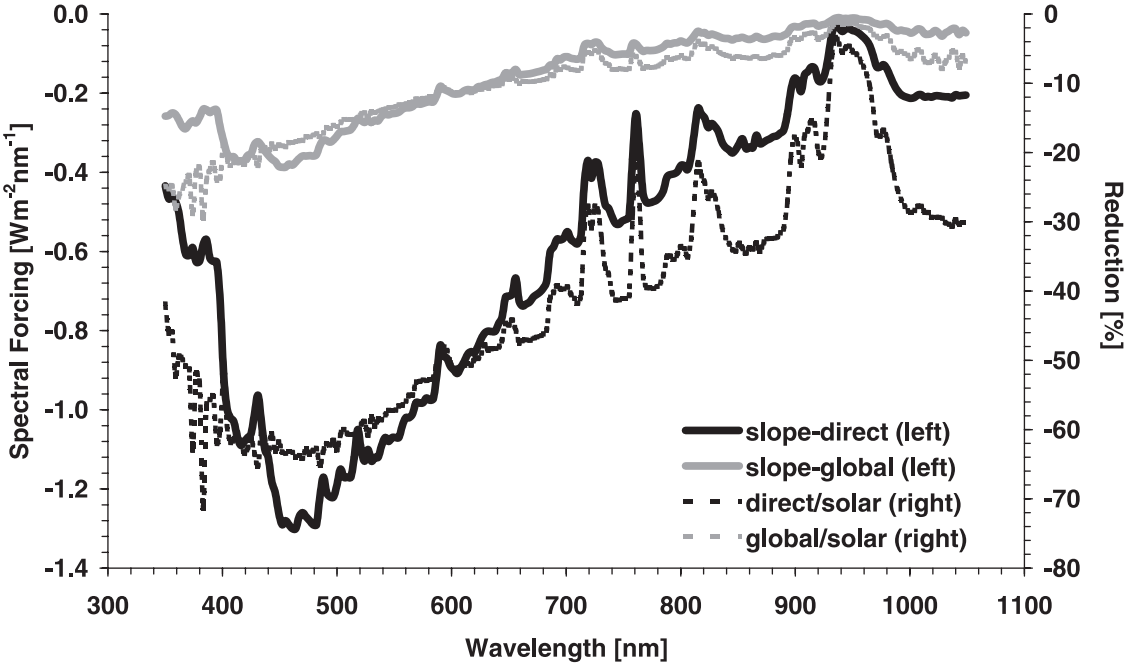

Figure 9. Spectral dependence of the forcing for the global and direct beam irradiance from ASD measurements between 350 and 1050 nm wavelengths. Solid lines: spectral forcing slopes, dashed lines: relative reduction of irradiance due to a unit increase in aerosol optical depth.

directly from the shape of the spectral slopes. Dividing those spectral slopes by the extraterrestrial irradiance yields to the relative reduction of solar irradiance due to a unit increase in optical depth at 500 nm for all spectral channels. This is plotted in Figure 9 (dashed black and gray lines, right axis) as percentage reduction of the spectral irradiance due to a unit increase in optical depth at 500 nm wavelength. The global irradiance is reduced most strongly (-25%) in the lower wavelengths around 350 nm due to the aerosols observed. This reduction in global irradiance asymptotically decreases to values of about -5% reduction above 1000 nm wavelength. The direct irradiance is also reduced strongly by the aerosols but in contrast to the global irradiance has a peak of reduction of -65% at 450 nm. The reduction in the direct irradiance for the wavelengths above 500 nm is asymptotically decreasing to values of about -30% at 1000 nm. The difference of these patterns clearly shows the importance of strong forward scattering at short wavelengths which apparently compensates for parts of the reduction in the global irradiance slope observed. The smaller influence of the aerosols (smaller slope values in the 400–700 nm or the 295–2900 nm range) observed in the global irradiance slope compared to the slope of the direct irradiance versus aerosol optical depth is mostly compensated by increased diffuse irradiance from wavelengths below 450 nm.

5. Discussion and Conclusion

[43] The aerosol optical depth, the aerosol forcing for different broad wavelength bands and the fully resolved spectral aerosol forcing have been derived from a variety of instruments from measurements onboard the *Ronald H. Brown* during IFP 99 of INDOEX.

[44] The study clearly demonstrates the application of the grating spectrometer for the aerosol forcing problem. Given the numerous recent studies on anomalous clear sky solar absorption [e.g., *Arking*, 1999; *Halthore et al.*, 1998], we need spectral measurements of the sort shown here to settle this dispute. *Satheesh and Ramanathan* [2000] show excellent agreement between model and observations for the aerosol forcing. However, we need to compare the models and observations on nanometer spectral resolution before settling this major controversy regarding anomalous absorption.

[45] The spectrometer used in this study has been factory calibrated before and after the cruise and frequently during the cruise by intercomparison with an optical standard light source. This way a small drift of the instruments response could be accounted for during the calibration procedure. The instruments cosine response has also been characterized before the cruise and an appropriate correction has been applied to the hemispherically integrated measurements. We have also corrected the observed direct spectral irradiance for Rayleigh attenuation and ozone absorption in the Chappuis band, using the in situ measured ozone columnar content from the ship. Intercomparison with other instruments on the same platform and from other platforms show an agreement between the different sources of spectral optical depth data, which is within the manufacturers stated accuracies and proof the reliability of the spectrometer data used and presented in this study. We also demonstrate that the spectrometer optical depths are consistent with sunphotometer data within the accuracy stated by the manufacturers of the respective instruments. Next we derive the forcing with full spectral resolution between pristine and polluted air masses. The differences decrease continuously from 350 nm wavelength to 1050 nm. The aerosol spectral

forcing peaks between 400 and 550 nm, in parts because aerosol optical depth is high, but also still weighted with the extraterrestrial irradiance. Dividing this spectral aerosol forcing by the extraterrestrial irradiance observed in each spectral channel leads to the percentage reduction in downwelling irradiance due to a unit increase in optical depth at 500 nm. The spectral global irradiance is most strongly effected in the lowest wavelengths (−25%) with decreasing values toward longer wavelengths (−5%) at 1000 nm. The direct beam's spectral reduction is about −40% at 350 nm, peaks at 450 nm with −65% and decreases toward longer wavelengths to reach values around −30% at 1000 nm.

[46] Our integrated forcing and spectral aerosol optical depth values quantified before compare to the results from TARFOX and ACE-2 in the following way: The direct radiative forcing has been estimated in the frame of TARFOX for the Atlantic off the coast of the United States. The approach to derive the direct forcing during TARFOX was quite different from the direct measurement approach presented in this paper. *Russell et al.* [1997b] took spectral optical depth measurements from 6-channel and 14-channel photometers to derive the aerosol size distributions. Together with refractive indices they estimated the spectral single scattering albedo, the asymmetry parameter and the spectral optical depth for the entire solar spectrum (300–3000 nm) and modeled the radiative fluxes. They find a direct aerosol forcing at the surface of −50 to −190 W m^{-2}, depending on the particular day for maximal optical depth values of up to 0.55 at mid-visible wavelengths in that geographical area. Their daily average values range from −60 to −90 W m^{-2} depending on some model assumptions made for the calculation and compare these with direct measurements from aircraft.

[47] During ACE-2, maximal optical depth values of up to 0.35 at 500 nm were found for air masses originating from the Iberian Peninsular corresponding with increased wavelength dependence. For the most pristine air masses they find optical depths of 0.03 at 500 nm with almost no spectral dependence [*Livingston et al.*, 2000].

[48] The maximum optical depths and their spectral dependence found during TARFOX are very close to the values we find in our study for the Arabian Sea and the Indian Ocean, while the maximum optical depths from ACE-2 do not reach such high values. The direct aerosol forcing found during TARFOX is comparable to the values we present here for INDOEX.

[49] **Acknowledgments.** We thank the crew of the *Ronald H. Brown* for making this cruise possible. The authors also wish to thank Francisco Valero and Sabrina Simpson of the Atmospheric Research Laboratory, Scripps Institution of Oceanography, University of California, San Diego, for facilitating the calibration laboratory for the angular calibration of the spectrometer. A. Jayaraman of the Physical Research Laboratory in Ahmedabad, India, supplied the optical depth measurements from the Sagar Kanya for intercomparison in this paper — thank you. This work was funded by the National Science Foundation (grant ATM9612887) and the Department of Energy (grant DE-FGO 3-91ER61198). Publication charges have been made available through GKSS Research Center, Geesthacht, Germany.

References

Arking, A., Bringing climate models into agreement with observations of atmospheric absorption, *J. Clim.*, *12*, 1589–1600, 1999.

Charlson, J. R., E. Schwartz, J. M. Hales, R. D. Cess, J. A. Coakley, J. E. Hansen, and D. J. Hofman, Climate forcing by anthropogenic aerosols, *Science*, *255*, 423–430, 1992.

Clarke, A. D., S. Howell, P. K. Quinn, T. S. Bates, J. A. Ogren, E. Andrews, and A. Jefferson, The INDOEX aerosol: A comparison and summary of microphysical, chemical and optical properties observed from land, ship and aircraft, *J. Geophys. Res.*, 10.1029/2001JD000572, in press, 2002.

Coakley, J. A., Jr., W. R. Tahnk, A. Jayaraman, P. K. Quinn, C. Devaux, and D. Tanre, Aerosol optical depths and direct radiative forcing for INDOEX derived from AVHRR: Theory, *J. Geophys. Res.*, *107*, 10.1029/2000JD000182, in press, 2002.

Curtiss, B., and A. F. H. Goetz, Field spectrometry: Techniques and instrumentation, in *FieldSpec User's Guide*, Analytical Spectral Devices Inc., Boulder, Colorado, 1997.

Dickerson, R. R., M. O. Andreae, T. L. Campos, O. L. Mayol-Bracero, C. Neususess, and D. Streets, Analysis of black carbon and carbon monoxide observed over the Indian Ocean: Implications for emissions and photochemistry, *J. Geophys. Res.*, *107*, 10.1029/2001JD000501, in press, 2002.

Fraser, R. S., and Y. J. Kaufman, The relative importance of aerosol scattering and absorption in remote sensing, *IEEE Trans. Geosci. Remote Sens.*, 625–633, GE-23(5), 1985.

Halthore, R. N., S. Nemesure, S. E. Schwartz, D. G. Imre, A. Berk, E. G. Dutton, and M. H. Bergin, Models overestimate diffuse clear-sky surface irradiance: A case for excess atmospheric absorption, *Geophys. Res. Lett.*, *25*, 3591–3594, 1998.

Intergovernmental Panel on Climate Change (IPCC), *Climate Change, 1994: Radiative Forcing of Climate Change and an Evaluation of IPCC IS92 Emission Scenarios*, 339 pp., Cambridge Univ. Press, New York, 1995.

Jayaraman, A., D. Lubin, S. Ramachandran, V. Ramanathan, E. Woodbridge, W. Collins, and K. S. Zalpuri, Direct observations of aerosol radiative forcing over the tropical Indian Ocean during the Jan–Feb 1996 pre-INDOEX cruise, *J. Geophys. Res.*, *103*, 13,827–13,836, 1998.

Jayaraman, A., S. K. Satheesh, A. P. Mitra, and V. Ramanathan, Latitude gradient in aerosol properties across the inter tropical convergence zone: Results from the joint Indo-US study onboard Sagar Kanya, *Current Science*, (supplement) *80*, 128–137, 2001.

Kiedron, P. W., J. J. Michalsky, J. L. Berndt, and L. C. Harrison, Comparison of spectral irradiance standards used to calibrate shortwave radiometers and spectroradiometers, *Appl. Opt.*, *38*, 2432–2439, 1999.

Kiehl, J. T., and B. P. Briegleb, The radiative roles of sulfate aerosols and greenhouse gases in climate forcing, *Science*, *260*, 311–314, 1993.

King, M. D., Y. J. Kaufman, D. Tanre, and T. Nakajima, Remote sensing of tropospheric aerosols from space: past, present and future, *Bull. Am. Meteorol. Soc.*, *80*(11), 2229–2259, 1999.

Kurucz, R. L., Synthetic infrared spectra, in *Infrared Solar Physics, International Astronomical Union Symposium 154*, edited by D. M. Rabin and J. T. Jefferies, 523–531, Kluwer, 1992.

Labs, D., and H. Neckel, The radiation of the solar photosphere from 2000 Å to 100 m, *Z. Astrophys.*, *69*, 1–73, 1968.

Leckner, B., The spectral distribution of solar radiation at the earths surface — elements of a model, *Sol. Energy*, *20*(2), 143–150, 1978.

Licor, *1800-02 Optical Radiation Calibrator: Instruction Manual, Licor Publ. 8508–44*, 1990.

Livingston, J. M., et al., Shipboard sunphotometer measurements of aerosol optical depth spectra and columnar water vapor during ACE-2, and comparison with selected land, ship, aircraft, and satellite measurements, *Tellus, Ser. B*, *52*, 594–619, 2000.

McCormick, P. H., and H. Sührcke, Cloud-Reflected Radiation, *Nature*, *345*, 773, 1990.

Meywerk, J., Influence of clouds on the spectral solar irradiance at the sea surface, Ph.D. thesis, Max-Planck Institute for Meteorology, Hamburg, Germany, Examensarbeit Nr. 45, May 1997, ISSN 0938-5177, 102 pp., 1997.

Meywerk, J., and V. Ramanathan, Observations of the spectral clear-sky aerosol forcing over the tropical Indian Ocean, *J. Geophys. Res.*, *104*, 24,359–24,370, 1999.

Michalsky, J. J., J. C. Liljegren, and L. C. Harrison, A comparison of sunphotometer derivations of total column water vapor and ozone to standard measures of the same at the Southern Great Plains atmospheric radiation measurement site, *J. Geophys. Res.*, *100*, 25,995–26,003, 1995.

Molina, L. T., and M. J. Molina, Absolute absorption cross sections of ozone in the 185 to 350 nm wavelength range, *J. Geophys. Res.*, *91*, 14,501–14,508, 1986.

Mühle, J., A. Zahn, C. A. M. Brenninkmeijer, V. Gros, and P. J. Crutzen, Air mass classification during the INDOEX R/V *Ronald Brown* cruise using measurements of nonmethane hydrocarbons, CH_4, CO_2, CO, ^{14}CO, and $\delta^{18}O(CO)$, *J. Geophys. Res.*, *107*, 10.1029/2001JD000730, in press, 2002.

Nguyen, H. V., S. M. Bhandari, A. Jayaraman, V. Ramanathan, L. V. G. Rao, S. T. Rupert, G. Viswanathan, S. F. Williams, and K. S. Zalpuri, *INDOEX 1998 First Field Phase Operation Summary, C4 Publ. 201*, INDOEX Project Off., La Jolla, California, Aug. 1998.

Penndorf, R., Tables of refractive index for standard air and Rayleigh scattering coefficient for the spectral region between 0.2 and 20 μm and their application to atmospheric optics, *J. Opt. Soc.*, *47*(2), 176–182, 1957.

Raes, F., T. Bates, F. McGovern, and M. van Liedekerke, The 2nd Aerosol Characterization Experiment (ACE-2): General overview and main results, *Tellus, Ser. B*, *52*, 111–125, 2000.

Ramanathan, V., et al., *Indian Ocean Experiment (INDOEX): A Multiagency Proposal for a Field Experiment in the indian Ocean*, C4 Publ. 162, Scripps Int. of Oceanogr., La Jolla, Calif., 1996.

Reagan, J., K. Thome, B. Herman, and R. Gall, Water vapor measurements in the 0.94 micron absorption band: calibration, measurement and data applications, in *Proceedings, International Geoscience and Remote Sensing Symposium*, Ann Harbor, 1987.

Russell, P. B., P. V. Hobbs, and L. L. Stowe, The Tropospheric Aerosol Radiative Forcing Observation Experiment (TARFOX), in *Proceedings of the A&WMA/AGU Speciality Conference on Visual Air Quality, Aerosols and Global Radiation Balance, Sept. 9–12, 1997*, Bartlett, N. H., 1997a.

Russell, P. B., P. Hignett, L. L. Stowe, J. M. Livingston, S. Kinne, and J. Wong, Direct aerosol radiative forcing: Calculation and measurements from the Tropospheric Aerosol Radiative Forcing Observational Experiment (TARFOX), in *Proceedings of the A&WMA/AGU Speciality Conference on Visual Air Quality, Aerosols and Global Radiation Balance, Sept. 9–12, 1997*, Bartlett, N. H., 1997b.

Satheesh, S. K., and V. Ramanathan, Large differences in tropical aerosol forcing at the top of the atmosphere and Earth's surface, *Nature*, *405*, 60–63, 2000.

J. Meywerk, GKSS Research Center, Institute for Coastal Research, Max-Planck-Str., 21502, Geesthacht, Germany. (Jens.Meywerk@gkss.de.)

V. Ramanathan, Center for Clouds, Chemistry, and Climate, Scripps Institution of Oceanography, University of California San Diego, La Jolla, USA.